IEEE Access
Multidisciplinary | Rapid Review | Open Access Journal

Received April 26, 2022, accepted May 29, 2022, date of publication June 9, 2022, date of current version June 14, 2022.

Digital Object Identifier 10.1109/ACCESS.2022.3181616

Motor Parametric Design Using an Electro-Hydraulic Model of a Brake System

SEON-YEOL OH[1], KYU-YUN HWANG[2], (Member, IEEE), BAIK-KEE SONG[2], AND SUNG-IL KIM[3], (Member, IEEE)

[1]Department of CAE, The Brake Research and Development Center, Mando, Bundang-gu, Seongnam-si 13486, South Korea
[2]Department of Mechanical Hardware 1-1, The Brake Research and Development Center, Mando, Bundang-gu, Seongnam-si 13486, South Korea
[3]Department of Electrical Engineering, Hoseo University, Asan-si, Chungcheongnam-do 31499, South Korea

Corresponding authors: Baik-Kee Song (songbk82@gmail.com) and Sung-Il Kim (kimsi@hoseo.edu)

This work was supported by the National Research Foundation of Korea (NRF) funded by the Korea Government (Ministry of Science and ICT) under Grant 2021R1F1A1061806

ABSTRACT Autonomous emergency braking (AEB) is one of the safety technologies of the integrated electronic brake (IEB) system and is critical to avoiding or mitigating vehicular collisions. In addition, a motor is a significant component of the IEB system for its actuation, and it greatly affects this system's performance under AEB. Notably, the determination of the IEB system's motor parameters without considering its performance under AEB will not satisfy its requirements, especially due to this system's hydraulic and electric complexity. In addition, the IEB system motor's dynamic characteristics have a significant impact on the AEB performance. They are also closely related to this motor's parameters, such as flux-linkage, inductance, and resistance. Therefore, this research performs the IEB system's motor parametric design corresponding to this system's necessary performance under AEB, using a coupled simulation model composed of this system's motor and hydraulic subsystems. First, the IEB system's motor and hydraulic subsystems are modeled in MATLAB/Simulink and AMESim, respectively, and the coupled simulation of these subsystems is performed in Simulink using their models. Second, the respective ranges of the IEB system's motor parameters corresponding to this system's necessary performance under AEB are determined from the above-mentioned coupled simulation, and their corresponding motor is designed using a finite element analysis in ANSYS Maxwell. Third, the IEB system's fabricated, parametric-designed motor is tested for standalone performance. Finally, the IEB system incorporated with the said parametric-designed motor is experimentally verified of its performance under AEB. Meanwhile, the respective simulated and experimental performances of the IEB system under AEB and its parametric-designed motor agree well. This agreement indicates that the IEB system's motor parametric design presented in this research, based on this system's coupled simulation model and finite element analysis on this model, is valid.

INDEX TERMS autonomous emergency braking (AEB), Brake, finite element analysis (FEA). inductance, integrated electronic brake (IEB), model-based design (MBD), motor parametric design, motor, resistance, simulation, surface-mounted permanent magnet (SPM),

I. INTRODUCTION

Currently, automotive companies worldwide attempt to minimize their energy consumption and improve energy efficiency due to the intensifying regulations limiting carbon dioxide emissions. Hence, the demand for electronic systems in the low-carbon dioxide-emitting electric vehicles (EVs), hybrid electric vehicles (HEVs), and plug-in HEVs (PHEVs) has substantially increased. Notably, conventional brake systems, which use a vacuum pump or booster to generate the braking pressure, have also been replaced with the (motor-driven) integrated electronic brake (IEB) system, as the IEB system is lightweight and operates on electricity only [1]–[4]. Hence, the IEB system's motor design studies have also increased [5], [6].

Many studies have designed a motor using finite element analysis (FEA). In particular, they examined a motor's performance in terms of its design parameters using FEA.

The associate editor coordinating the review of this manuscript and approving it for publication was Qinfen Lu.

For example, S. -I. Kim *et al.* [7] used FEA to obtain the back-EMF of an internal permanent magnetic synchronization motor (IPMSM) that satisfied this motor's efficiency requirement. Further, Y. K. Chin *et al.* [8] investigated the effect of a motor's geometric parameters on its performance using FEA and compared this motor's FEA and test cogging torques. Likewise, Ali Sarikhani *et al.* [9] presented an FEA-based design optimization for permanent magnet (PM) motors. Finally, Chang *et al.* [10] used FEA to calculate the saturation factor of linear motors. However, FEA is difficult in studying the performance of the IEB system, even though it is beneficial in this system's motor design. In order to find this motor's optimum design parameters for achieving excellent performance of this system, the evaluation of IEB system performance is a priority.

The IEB system can implement pivotal vehicle safety technologies such as anti-lock brake system (ABS), electronic stability control (ESC), autonomous emergency braking (AEB), adaptive cruise control (ACC), etc. Meanwhile, model-based design (MBD), which utilizes a simulation model of a system's digital prototype, is useful in examining the IEB system's safety performance [11], [12]. For example, D. Tavernini *et al.* [13] proposed an explicit nonlinear model predictive controller (eNMPC) for the antilock braking system (ABS) operating through the IEB system. They used the Hardware-in-the-Loop (HiL)'s vehicle simulation model to simulate this controller's performance. Likewise, X. He *et al.* [14] proposed an AEB control strategy for the IEB system, using the radial basis function (RBF) network control arithmetic that considered uncertainty and nonlinearity, and verified the proposed strategy's performance using a coupled simulation under MATLAB/Simulink and AMESim. The MBD method was also effectively used in developing control logic apart from the above-mentioned applications in the IEB system performance predictions [15]–[18]. However, only a few studies used the MBD method to identify the IEB system's motor parameters corresponding to this system's necessary performance. Notably, X. Yang, J. Li, and others [19], [20] analyzed the IEB system's dynamic performance according to this system's structural parameters, such as motor shaft inertia and solenoid valves' throttle orifice diameter, using a simulation model.

As can be seen from the studies mentioned above, the simulation model of the IEB system was mainly used to develop the control logic applied to the safety performances, and there was little use of the simulation model for motor design. However, this research uses the MBD method for the parametric design of the IEB system's motor, corresponding to this system's necessary performance under AEB. Thus, we propose an IEB system model that can be simulated to find the respective ranges of the IEB system's motor parameters corresponding to this system's said necessary performance. Then, the motor corresponding to these motor parameters' ranges is parametrically designed using FEA. Finally, this parametric-designed motor and the IEB system incorporated with it are studied under simulation and experiment, respectively, and the simulated and experimental results are compared.

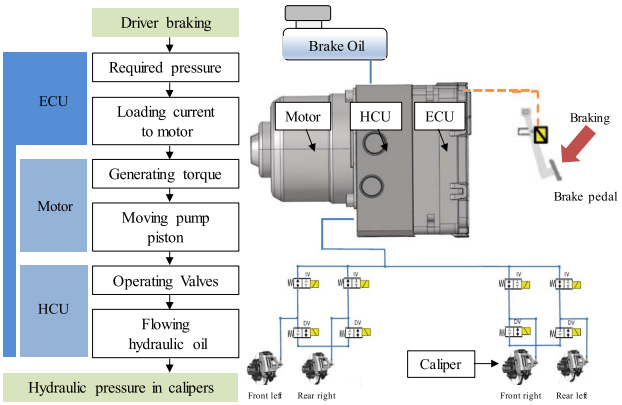

FIGURE 1. The IEB system and its operating sequence.

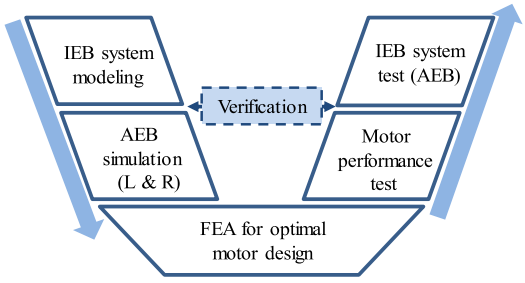

FIGURE 2. The IEB system's motor parametric design flowchart.

II. THE IEB SYSTEM'S PRINCIPLE

As shown in Fig. 1, The IEB system consists of a hydraulic circuit unit (HCU), an electric control unit (ECU), and a motor. Generally, the IEB system's operating sequence is as follows. First, the ECU supplies an electric current to the motor to generate the appropriate high pressure of the brake fluid inside the HCU's hydraulic pump, according to the brake pedal movement when the driver presses the brake pedal. Notably, the motor's rotational motion is converted into a linear forward motion of the said hydraulic pump's piston, delivering the high-pressure brake fluid to each wheel's calipers for braking. Finally, the ECU reduces its supply of electric current to the motor for the reduced pressure of the brake fluid inside the HCU's hydraulic pump when the driver releases pressure on the brake pedal. Meanwhile, this hydraulic pump's piston moves backward under this release of pressure on the brake pedal [21].

III. THE IEB SYSTEM'S MOTOR PARAMETRIC DESIGN FLOWCHART

The IEB system motor must be appropriate for this system's necessary performance under AEB. In particular, the IEB system must achieve the necessary build-up rate of the brake fluid pressure under AEB, which indicates how faster this system applies braking pressure to the wheels for AEB. Likewise, the IEB system supplies the maximum current to the

TABLE 1. The IEB system's motor requirements.

Parameter	Value
Motor type	Surface-mounted Permanent Magnet Synchronous Motor (SPMSM)
Poles / Slots	8 / 12
Maximum torque	4.4 Nm

motor in a short time under AEB. Subsequently, the motor is required to generate corresponding maximum power, ideally during this short time, to apply braking pressure to the wheels quickly. Therefore, this research follows the motor parametric design flowchart given in Fig. 2, which is based on the strategies adopted in software validation and verification [22]. The design sequence in this flowchart is as follows. (1) The IEB system's motor and hydraulic subsystems are modeled in MATLAB/Simulink and AMESim, respectively. Later, the IEB system model is created in Simulink by coupling these subsystem models and appending this system's power source, resistances of the harness, and ECU to them. (2) The respective ranges of the IEB system's motor parameters (only this motor's inductance and resistance) corresponding to this system's necessary performance under AEB are determined from the coupled simulation on the IEB system model. On the other hand, this motor's flux-linkage is predetermined by the hydraulic pump dimensions and maximum brake fluid pressure. (3) The IEB system's motor parametric design, corresponding to the respective ranges of these parameters (from the above-mentioned coupled IEB system simulation), is carried out using FEA in ANSYS Maxwell. In particular, this design considers the said motor's stator dimensions and the number of coil turns as variables. (4) The IEB system's parametric-designed motor is fabricated and experimentally verified of its performance. (5) The performance of the IEB system incorporated with its parametric-designed motor under AEB is studied through the coupled simulation and an experiment.

IV. THE IEB SYSTEM MODELING

This research develops an integrated IEB system model, considering the electric current control logic for its performance under AEB as follows.

A. THE IEB MOTOR SUBSYSTEM MODEL

The IEB system motor used in this research is an 8-pole, 12-slot surface-mounted permanent magnet synchronous motor (SPMSM). This motor's specifications are listed in Table 1. Notably, the IEB system's maximum required motor torque is decided by its maximum brake fluid pressure and the hydraulic pump's piston diameter.

Meanwhile, the maximum IEB system current is determined by the current capacity of its ECU inverter's field effective transistor (FET) element. The respective torque and voltage equations of the IEB system motor in the d- and q- coordinate systems are as follows:

$$V_d = RI_d + L_d \frac{dI_d}{dt} - \omega L_q I_q \tag{1}$$

$$V_q = RI_q + L_q \frac{dI_q}{dt} + \omega L_d I_d + \omega \psi_m \tag{2}$$

$$T_e = \frac{3}{2} P_n \psi_m I_q \tag{3}$$

where L_d and L_q are the inductances in the d- and q- coordinates, respectively (they are equal for the SPMSM); R is the resistance; V_d and V_q are the voltage components in the d- and q- coordinates, respectively; I_d and I_q are the currents in the d- and q- coordinates, respectively; ψ_m is the maximum flux-linkage; ω is the electrical angular velocity of the rotor; T_e is the motor torque; P_n is the number of pole pairs.

Equations (1) - (3) show that the IEB motor subsystem model can be built based on its following motor parameters: inductance, resistance, and flux-linkage. However, the IEB system motor's flux-linkage is decided by its maximum torque, current, and polar pairs, which are predetermined. So, this research considers only this motor's inductance and resistance in the IEB motor subsystem model and determines their respective ranges for the IEB system's necessary performance under AEB through simulation. In particular, this determination considers the IEB system motor's stator dimensions (length and diameter) and coil winding characteristics (number of coil turns) as variables.

Notably, Fig. 3 (a) shows that the IEB motor subsystem's current controller develops V_d and V_q, which supply their corresponding currents to the IEB system motor, through an ECU inverter switching based on space vector pulse width modulation (SVPWM). In addition, Fig. 3 (b) shows the PI control logic of the above-mentioned current controller. In particular, this PI control logic is based on a closed-loop control (including feedback and feedforward controls) developing voltages V_d and V_q for the supply of the target currents: I_d and I_q, respectively, to the IEB system motor. Finally, the IEB system motor's back EMF and the cross-coupled components that depend on its speed are considered in its feedforward compensation. Meanwhile,

$$K_p = L_d \omega_{cc} \tag{4}$$

$$K_i = R\omega_{cc} \tag{5}$$

where K_p and K_i are the IEB system motor's proportional and integral gains, respectively; ω_{cc} is the cut-off frequency.

Notably, the IEB system motor's proportional and integral gains (including its resistance and inductance), given respectively in Equations (4) and (5), are inputted to the IEB motor subsystem's PI controller. Since these gains are needed to follow the command current while reducing the error between the command and measured currents during feedback control, the IEB system motor's inductance and resistance affect its dynamic characteristics. These dynamic characteristics, in turn, affect the IEB system's performance under AEB, as mentioned earlier. Accordingly, the IEB system motor's

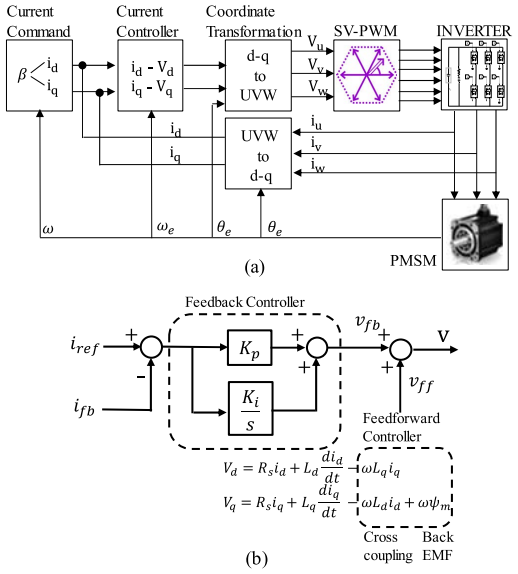

FIGURE 3. (a) The IEB motor subsystem and (b) its PI control logic.

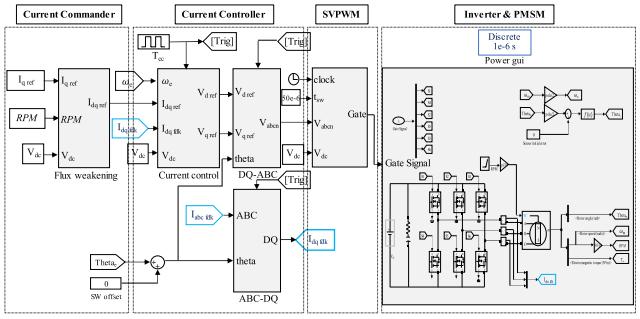

FIGURE 4. The IEB motor subsystem model created in MATLAB/Simulink.

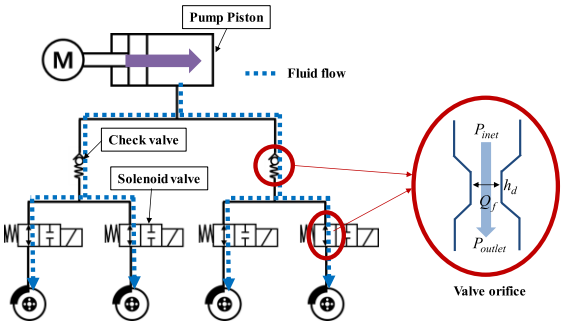

FIGURE 5. The conceptual diagram of hydraulic subsystem and one of its valve orifices.

inductance and resistance are the primary parameters in its design under the present research.

Meanwhile, its flux-linkage also affects its performance through torque.

Figure 4 shows the IEB motor subsystem model created in MATLAB/Simulink, considering all of this subsystem's components mentioned above. In addition, this motor's mechanical loss constant, reflecting the mechanical loss between its shaft and bearings due to its rotation, is obtained

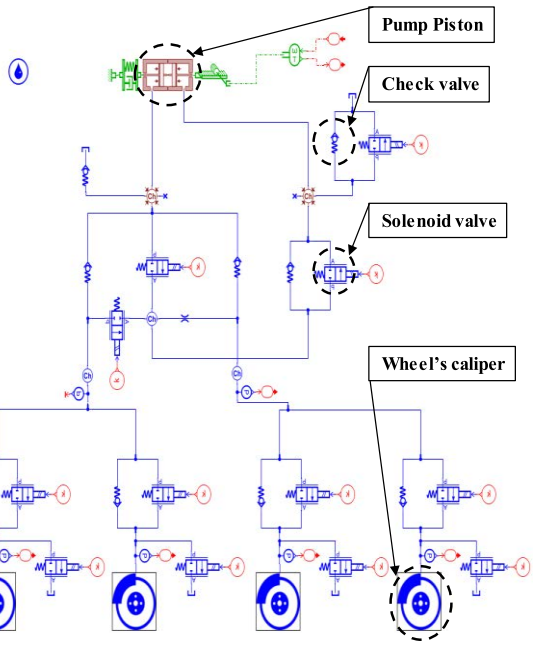

FIGURE 6. The IEB hydraulic subsystem model created in AMESim.

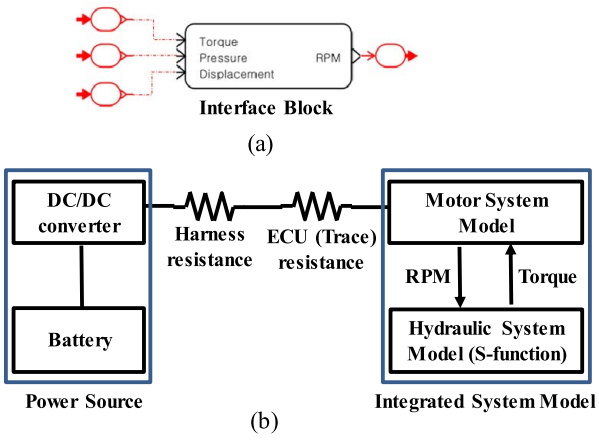

FIGURE 7. The IEB system's (a) interface block and (b) model and power source in MATLAB/Simulink.

from an experiment and inputted to the IEB motor subsystem model. In particular, the IEB system motor's mechanical loss and mechanical loss constant are related as follows.

$$T_{MLoss} = K_{MLoss} \times RPM \tag{6}$$

where T_{MLoss} is the mechanical loss; K_{MLoss} is the mechanical loss constant: equal to 0.000038 (Nm/*RPM*) for the SPMSM used in this research; *RPM* is the angular velocity (expressed in revolutions per minute) of this motor.

B. THE IEB HYDRAULIC SUBSYSTEM MODEL

The IEB hydraulic subsystem includes a hydraulic pump, converting the force induced on its piston by the IEB system motor to its brake fluid pressure in the wheels' calipers through HCU, and many check and solenoid valves, as shown in Fig. 5. In particular, the check valves block the brake

fluid's backflow and allow this fluid's flow in the forward direction. On the other hand, the solenoid valves are electrically controlled and affect the brake fluid's flow by using an electromagnetic coil that opens and closes these valves. Meanwhile, a highly reliable IEB hydraulic subsystem must compute its brake fluid's respective pressure drops and flow rates across the orifices of the valves on this fluid's flow path accurately. So, precisely calculating the flow coefficient, relating the above-mentioned brake fluid's pressure drop across any of the said valve orifices and the corresponding flow rate [23], is essential in achieving a highly reliable IEB hydraulic subsystem. Notably, the flow rate and pressure drop of the IEB hydraulic subsystem's brake fluid across any of the above-mentioned valve orifices are obtained using the following equations.

$$Q_f = c_q \sqrt{\frac{2\Delta P}{\rho}} A_c \tag{7}$$

$$c_q = c_{q\max} \tanh\left(\frac{2\lambda}{\lambda_{crit}}\right) \tag{8}$$

$$\lambda = \frac{\rho h_d}{\mu}\sqrt{\frac{2\Delta P}{\rho}} \tag{9}$$

$$E = \rho \frac{dP}{d\rho} \tag{10}$$

where Q_f is this brake fluid's flow rate across the orifice; A_c is the orifice's cross-sectional area; ΔP is this brake fluid's pressure drop across the orifice; ρ is this brake fluid's density; c_q is the coefficient of this brake fluid's flow across the orifice; $c_{q\,max}$ is the maximum of the coefficient of this brake fluid's flow across the orifice; λ is the number of this brake fluid's flow across the orifice; λ_{crit} is the critical number of this brake fluid's flow across the orifice; h_d is the orifice diameter; μ is this brake fluid's absolute viscosity; E is this brake fluid's bulk modulus.

Notably, it is important that the IEB hydraulic subsystem modeling uses reliable maximum flow coefficient, critical flow number, and properties: fluid density, absolute viscosity, and bulk modulus related to this subsystem's brake fluid and its flow across the orifices of the valves in its flow path. Thus, these compressible brake fluid's properties are obtained from a property experiment. The corresponding maximum flow coefficient and critical flow number mentioned above are found from a computational fluid dynamics (CFD) analysis using STAR CCM+. Notably, this brake fluid's volume and density change according to its pressure (developed by the piston of the IEB hydraulic subsystem's hydraulic pump) due to this fluid's compressibility. Meanwhile, Fig. 6 shows the IEB hydraulic subsystem model created in AMESim, based on the above-mentioned aspects of this subsystem. Notably, all the above-mentioned check and the solenoid valves are kept open during the IEB system's operation under AEB to generate brake fluid pressure in the wheels' calipers quickly.

TABLE 2. The IEB system performance requirements under AEB for a battery voltage of 14 V.

The IEB system's respective brake fluid pressure range in the wheels' calipers	The IEB system requirement (this system's brake fluid pressure build-up rate)
0 → 2.5 MPa (from 0 MPa to 2.5 MPa)	≥ 25 MPa/s
0 → 5 MPa (from 0 MPa to 5 MPa)	≥ 35 MPa/s
0 → 10 MPa (from 0 MPa to 10 MPa)	≥ 42.5 MPa/s
0 → 14 MPa (from 0 MPa to 14 MPa)	≥ 45 MPa/s

C. THE INTEGRATED IEB SYSTEM MODEL

The IEB motor and hydraulic subsystem models developed are integrated in Simulink. Notably, this integration requires the conversion of the IEB hydraulic subsystem model (built in AMESim) to a system function (S-function) that can interact with the Simulink engine after defining the interface block (Fig. 7 (a))'s ports. Figure 7 (b) shows the IEB system model integrated in Simulink, with its power source, resistances of the harness, and ECU appended to this integration. In particular, the IEB system power source, consisting of a battery and a DC/DC converter, applies a constant voltage to the IEB motor subsystem. Likewise, this system's resistances of the harness and ECU are found from an experiment to precisely compute the voltage drop across the DC/DC converter and the IEB motor subsystem. In addition, the information communicated between the IEB motor and hydraulic subsystem models is only the IEB system motor's torque and RPM (Fig. 7 (a)), as the integrated IEB system model is intended for its performance simulation under AEB only. Finally, the interface block's ports collect the information on the piston displacement of the IEB system hydraulic pump and this system's brake fluid pressure in the wheels' calipers to complete the integrated IEB system's performance simulation.

V. THE RESPECTIVE RANGES OF THE IEB SYSTEM'S MOTOR PARAMETERS CORRESPONDING TO THIS SYSTEM'S NECESSARY PERFORMANCE UNDER AEB

We use the integrated IEB system model to find the respective ranges of this system's motor parameters (inductance and resistance) corresponding to this system's necessary performance under AEB. In particular, these ranges are found based on the IEB system's different required brake fluid pressure build-up rates through a parametric study.

Table 2 shows the IEB system performance requirements under AEB for a battery voltage of 14 V. Figure 8 gives the results of this parametric study. Notably, the respective ranges for the IEB system's motor parameters corresponding to this system's necessary performance under AEB are determined from the results as 30∼45 μH for inductance and 8∼9.8 mohm for resistance, by superimposing all these ranges given in Figs. 8 (a) - (d).

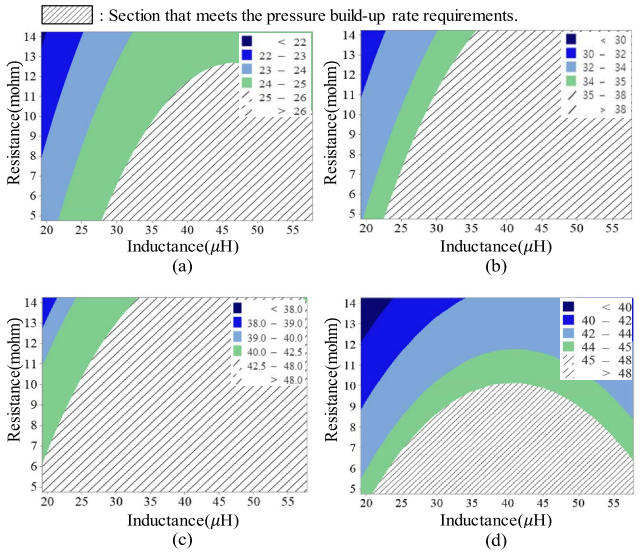

FIGURE 8. The IEB system's brake fluid pressure build-up rate under AEB for a respective brake fluid pressure range in the wheels' calipers equal to (a) 0 → 2.5 MPa, (b) 0 → 5 MPa, (c) 0 → 10 MPa, and (d) 0 → 14 MPa.

VI. THE IEB SYSTEM'S MOTOR PARAMETRIC DESIGN

The IEB system's motor parametric design, giving this motor's teeth and yoke thicknesses, stack length, and the number of coil turns, is carried out using FEA in ANSYS Maxwell. For the Maxwell analysis, a two-dimensional motor model is used. In order to increase accuracy, manufacturing tolerance of each component and stacking factor are considered. The electrical steel sheet for stator and rotor are 50A470 and 50A1300, respectively. The N44UH grade permanent magnet is used for drive magnets.

In particular, this design is performed with the ranges of this motor's parameters (obtained from the previous analysis) that correspond to the IEB system's necessary performance under AEB. Notably, the criteria for determining the detailed dimensions of this motor's stator are the magnetic flux density, flux-linkage, inductance, and resistance. In particular, the outer diameter of this stator is determined by the packaging limitations of the IEB system, and its inner diameter is predetermined by the piston size of this system's hydraulic pump. Meanwhile, this motor's air gap is 0.7 mm. Finally, this motor's coil diameter is decided by the current density in this coil, and this motor's slot fill factor is 43%.

Figure 9 (a) shows the IEB system's motor parametric design process for determining this motor's detailed stator dimensions, inductance, and resistance. In particular, the teeth and yoke thicknesses of the IEB system motor's stator are determined by the flux density at the center of its teeth and yoke, respectively. Notably, Fig. 9 (b) shows that the flux densities at the center of the said teeth and yoke (points A and B) are 1.7∼1.8 T and 1.3∼1.4 T, respectively, while the motor is loaded with maximum current. The flux densities are criteria to limit the magnetic saturation of the motor stator. Excessive magnetic saturation is limited because it negatively affects core loss, back-EMF, coaching torque, and torque ripple. [24], [25].

TABLE 3. The dimensions of the IEB system's parametric-designed motor from FEA, corresponding to this motor's different number of coil turns.

The IEB system motor's number of coil turns	16.5	17.5	18.5	19.5	20.5
Required area per slot for the IEB system motor's coil winding (mm^2)	94.13	99.8	105.5	111.2	116.0
Teeth thickness (mm)	5.9	6	6.1	6.2	6.3
Yoke thickness (mm)	4.35	4.4	4.5	4.6	4.7
Available area per slot for the IEB system motor's coil winding (mm^2)	108.8	111.7	112.7	112.1	107.9
Stack length (mm)	35.7	34.2	32	30.5	28.8
Resistance (mΩ)	8.98	9.37	9.36	9.57	9.70
Inductance (μH)	31.4	34.2	35.2	38.5	41.2

Table 3 shows the dimensions of the IEB system's parametric-designed motor from the FEA, corresponding to this motor's different number of coil turns. In particular, the teeth and yoke thicknesses of this motor's stator must be increased with this motor's number of coil turns to maintain the corresponding coil magnetic saturation within the corresponding prescribed limit. Likewise, the required area per slot for this motor's coil winding rises with the increasing number of coil turns. In contrast, the available area per slot for the same coil winding reduces with the same increasing number of coil turns due to a corresponding increase in the teeth and yoke thicknesses. Further, the stack length of the IEB system motor is determined to achieve its necessary flux-linkage after determining the above-mentioned teeth and yoke thicknesses. Finally, this motor's inductance and resistance are found with its finalized number of coil turns and stator dimensions.

Figure 10 shows the required and available areas per slot for the IEB system motor's coil winding in terms of this motor's number of coil turns. Notably, the said required area is less than the corresponding available area when this motor's number of coil turns is less than 19.5.

But, this motor's respective resistances corresponding to 16.5 and 17.5 coil turns don't result in the IEB system's necessary performance under AEB (given by the hatched section in Fig. 11). So, only the IEB system motor with 18.5 or 19.5 coil turns can be manufactured.

Further coupled simulations are conducted to compare the IEB system's performance under AEB with this system's motor having 18.5 and 19.5 coils turns, respectively. These simulations show that the IEB system's said performance is better with this system's motor having 19.5 coil turns compared to the one corresponding to 18.5 coil turns. Hence, the IEB system's motor parametric design is concluded by finding this motor's detailed dimensions corresponding to 19.5 coil turns in this motor. Consequently, this parametric-designed motor's resistance and inductance are 9.57 mohm

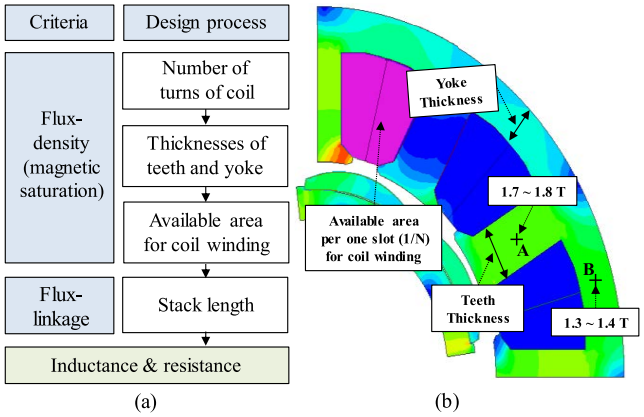

FIGURE 9. The IEB system's (a) motor parametric design process for determining this motor's stator dimensions, inductance, and resistance and (b) motor FEA results used in this motor's parametric design.

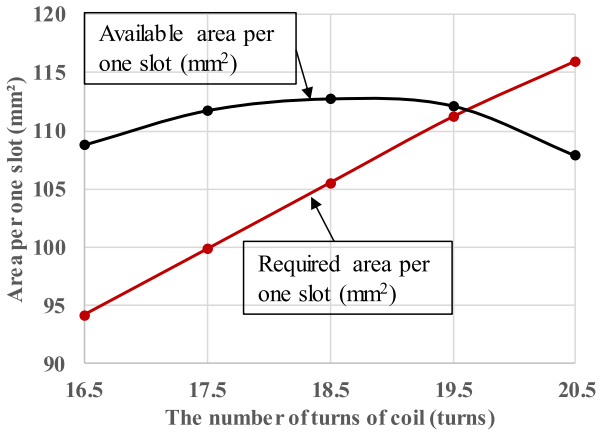

FIGURE 10. The required and available areas per slot for the IEB system motor's coil winding, in terms of this motor's number of coil turns.

TABLE 4. The parameters of the IEB system's parametric-designed motor.

Parameter	Value
Number of coil turns	19.5
Resistance (mΩ)	9.57
Inductance (μH)	38.5
Flux-linkage (Wb)	0.0064

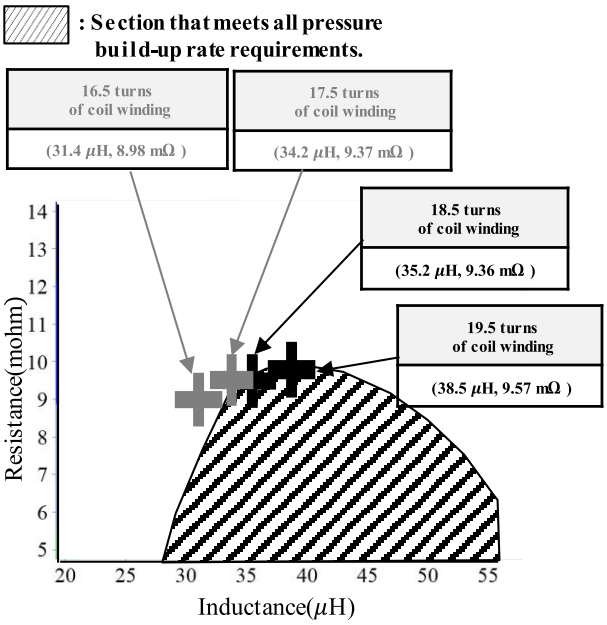

FIGURE 11. The IEB system's brake fluid pressure build-up rate for a respective brake fluid pressure range (combining all the corresponding individual ranges given above) in the wheel's calipers, in terms of its motor's number of coil turns.

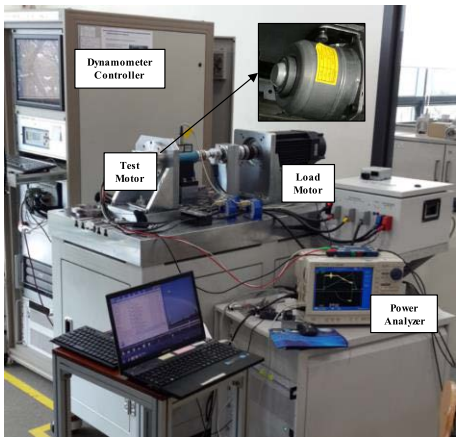

FIGURE 12. The motor test bench for the experimental-performance verification of the IEB system's parametric-designed motor.

and 38.5 μH, respectively. Table 4 gives these parametric-designed motor's parameters.

VII. RESPECTIVE EXPERIMENTAL-PERFORMANCE VERIFICATION OF THE IEB SYSTEM AND ITS PARAMETRIC-DESIGNED MOTOR

A. EXPERIMENTAL-PERFORMANCE VERIFICATION OF THE IEB SYSTEM'S PARAMETRIC-DESIGNED MOTOR

The IEB system's parametric-designed motor is fabricated, and its performance is verified experimentally. Figure 12 shows the motor test bench for this experimental-performance verification, consisting of a dynamometer controller, a power analyzer, the IEB system's parametric-designed motor under test, and a load motor. Notably, this experiment is performed at two different applied voltages under the same maximum current condition, as indicated in Table 5. Subsequently, the experimentally observed performance of the said parametric-designed motor is compared with the corresponding Simulink-simulated performance. This comparison shows a good agreement between these simulated and experimental performances, as shown in Fig. 13. Notably, the IEB system's fabricated, parametric-designed motor generates the required torque of 4.4 Nm at 1000 RPM.

TABLE 5. The input power and current for the experimental-performance verification of the IEB system's parametric-designed motor.

Test case	Case 1	Case 2
Motor line to line voltage (V_{peak})	10.5	12.5
Motor phase current (A_{peak})	120	

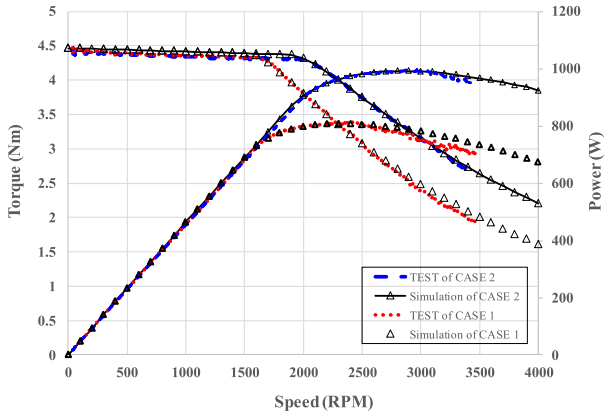

FIGURE 13. The simulated and experimental performances of the IEB system's parametric-designed motor.

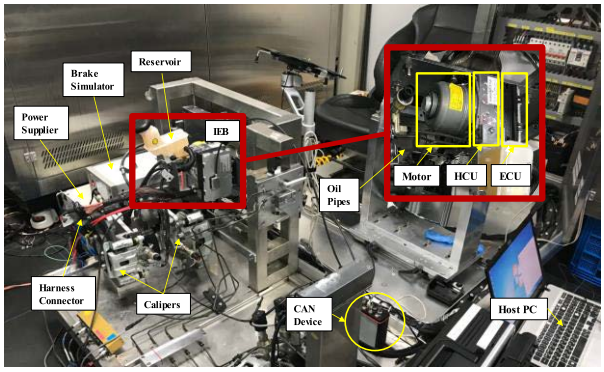

FIGURE 14. The IEB system test bench for the experimental-performance verification of the IEB system (incorporated with its parametric-designed motor) under AEB.

B. EXPERIMENTAL-PERFORMANCE VERIFICATION OF THE IEB SYSTEM (INCORPORATED WITH ITS PARAMETRIC-DESIGNED MOTOR) UNDER AEB

The performance of the IEB system (incorporated with its parametric-designed motor) under AEB is verified experimentally. Figure 14 shows the IEB system test bench, consisting of calipers, a reservoir, oil pipes, and a harness connector. In addition, a personal computer (PC), a CAN bus network, a brake simulator, and a power supplier are needed to operate this test bench and obtain the information of experimental-performance results. Notably, a voltage of 14V is applied to the IEB system by the power supply in this experiment.

Figure 15 shows the results of this experimental-performance verification. It also compares the respective IEB system-under-test's simulated and experimental brake fluid pressure build-up rates for different brake fluid pressure ranges at the wheels' calipers. Notably, the corresponding simulation and experiment show, respectively, that the IEB system's necessary performance under AEB is achieved for all the above-mentioned pressure ranges. In addition, Fig. 16 shows the IEB system (incorporated with its parametric-designed motor)'s simulated and experimental performances under AEB in terms of this system's operation information: the motor current, motor speed, hydraulic pump piston displacement, and brake fluid pressure at any wheel's caliper over time. Overall, these simulated and experimental responses show a good agreement, proving the effectiveness

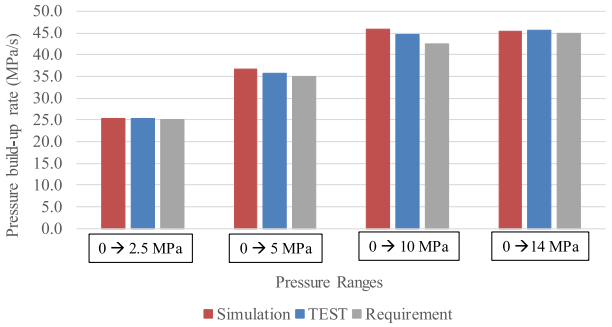

Range	Requirement	Simulation	Test	Result
0→2.5 MPa	≥ 25 MPa/s	25.3 MPa/s	25.2 MPa/s	PASS
0→5 MPa	≥ 35 MPa/s	36.8 MPa/s	35.7 MPa/s	PASS
0→10 MPa	≥ 42.5 MPa/s	45.9 MPa/s	44.6 MPa/s	PASS
0→14 MPa	≥ 45 MPa/s	45.4 MPa/s	45.7 MPa/s	PASS

FIGURE 15. The simulated and experimental performances of the IEB system (incorporated with its parametric-designed motor) under AEB, in terms of this system's brake fluid pressure build-up rate for different respective brake fluid pressure range at the wheels' calipers.

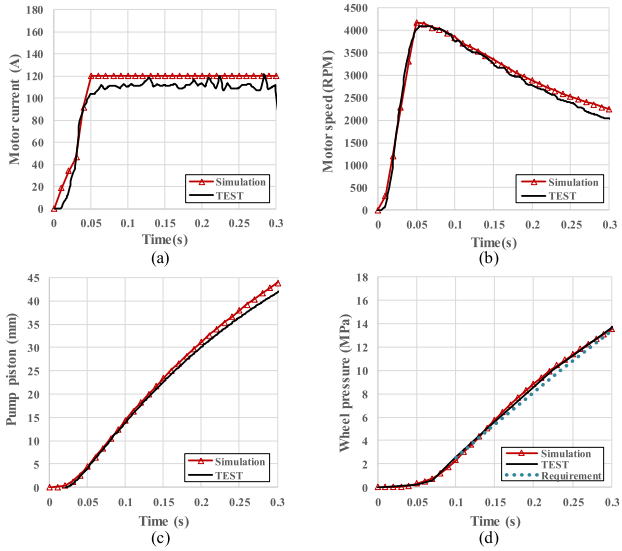

FIGURE 16. The IEB system (incorporated with its parametric-designed motor)'s simulated and experimental performances under AEB, in terms of this system's (a) motor current (b) motor speed (c) hydraulic pump piston displacement, and (d) brake fluid pressure at any wheel's caliper over time.

of the integrated IEB system model and simulation established in this research.

VIII. CONCLUSION

This research develops an integrated IEB system model for this system's motor parametric design under AEB. Notably, a highly reliable IEB system model is developed by integrating this system's motor subsystem model (including this subsystem's current controller and ECU inverter) and hydraulic subsystem model (built using this subsystem's brake fluid properties and the corresponding flow coefficients obtained from an experiment and CFD analysis, respectively). Subsequently, a coupled simulation of the IEB system model gives the respective ranges of the IEB system's motor parameters corresponding to this system's necessary performance under AEB. Further, this system's motor parametric design is carried out within these ranges. The parametric-designed motor is then fabricated and experimentally verified of its performance. Notably, this motor's respective simulated and experimental performances agree well, indicating the high reliability of the IEB motor subsystem model. Likewise, the IEB system (incorporated with its parametric-designed motor)'s performance under AEB is studied through simulation and experiment, respectively. The corresponding simulated and experimental performances of the IEB system also agree well, demonstrating the high reliability of the IEB system and the IEB hydraulic subsystem models. In addition, these results indicate that the MBD method used in this research for the IEB system's motor parametric design is effective. Therefore, the high-reliability IEB system model developed and verified in this research can be used in the future for this system's motor parametric design under reduced time and changing performance requirements of this system with the vehicle type. Also, it is expected that this proposed method of IEB system's motor parametric design will be more beneficial compared to other methods when this system becomes more complicated and difficult in the future.

REFERENCES

[1] X. Wang, X. Wu, S. Cheng, J. Shi, X. Ping, and W. Yue, "Design and experiment of control architecture and adaptive dual-loop controller for brake-by-wire system with an electric booster," *IEEE Trans. Transport. Electrific.*, vol. 6, no. 3, pp. 1236–1252, Sep. 2020.

[2] Z. Zhu, X. Wang, J. Yan, L. Li, and Q. Wu, "A dynamic decoupling control method for PMSM of brake-by-wire system based on parameters estimation," *IEEE/ASME Trans. Mechatronics*, early access, Dec. 22, 2021, doi: 10.1109/TMECH.2021.3130907.

[3] C. Li, C. He, Y. Yuan, and J. Zhang, "Co-simulation on performance evaluation of a new electronic control hydraulic braking system," in *Proc. IEEE 3rd Adv. Inf. Technol., Electron. Autom. Control Conf. (IAEAC)*, Oct. 2018, pp. 2500–2504.

[4] C. Riese, A. Verhagen, S. Schroeter, and F. Gauterin, "Comparison of a state of the art hydraulic brake system with a decentralized hydraulic brake system concept for electric vehicles," SAE Tech. Paper, 2017-01-2515, 2017.

[5] K. Y. Hwang and B.-I. Kwon, "Design of low-cost BLAC motors for integrated electric brake systems," *IEEE Access*, vol. 7, pp. 184183–184193, 2019.

[6] B.-K. Song, J.-W. Chin, D.-M. Kim, K.-Y. Hwang, and M.-S. Lim, "Temperature estimation using lumped-parameter thermal network with piecewise stator-housing modules for fault-tolerant brake systems in highly automated driving vehicles," *IEEE Trans. Intell. Transp. Syst.*, vol. 22, no. 9, pp. 5819–5832, Sep. 2021.

[7] S. I. Kim, G. H. Lee, J. P. Hong, and T. U. Jung, "Design process of interior PM synchronous motor for 42-V electric air-conditioner system in hybrid electric vehicle," *IEEE Trans. Magn.*, vol. 44, no. 6, pp. 1590–1593, Jun. 2008.

[8] Y. K. Chin and J. Soulard, "A permanent magnet synchronous motor for traction applications of electric vehicles," in *Proc. IEEE Int. Electr. Mach. Drives Conf.*, vol. 2, Jun. 2003, pp. 1035–1041.

[9] A. Sarikhani and O. A. Mohammed, "HIL-based finite-element design optimization process for the computational prototyping of electric motor drives," *IEEE Trans. Energy Convers.*, vol. 27, no. 3, pp. 737–746, Sep. 2012.

[10] J. Chang, D. H. Kang, I.-A. Viorel, and S. Larisa, "Transverse flux reluctance linear motor's analytical model based on finite-element method analysis results," *IEEE Trans. Magn.*, vol. 43, no. 4, pp. 1201–1204, Apr. 2007.

[11] J. Friedman, "MATLAB/Simulink for automotive systems design," in *Proc. Design Autom. Test Eur. Conf.*, Jul. 2006, pp. 1–2.

[12] K. Patil, M. Muli, and Z. Zhu, "Model-based development and production implementation of motor drive controller for hybrid electric vehicle," SAE Tech. Paper, 2013-01-0158, 2013.

[13] D. Tavernini, F. Vacca, M. Metzler, D. Savitski, V. Ivanov, P. Gruber, A. E. Hartavi, M. Dhaens, and A. Sorniotti, "An explicit nonlinear model predictive ABS controller for electro-hydraulic braking systems," *IEEE Trans. Ind. Electron.*, vol. 67, no. 5, pp. 3990–4001, May 2020.

[14] X. He, K. Yang, X. Ji, and Y. Liu, "Autonomous emergency braking control based on hierarchical strategy using integrated-electro-hydraulic brake system," SAE Tech. Paper, 2017-01-1964, 2017.

[15] B. Boazzo and G. Pellegrino, "Model-based direct flux vector control of permanent-magnet synchronous motor drives," *IEEE Trans. Ind. Appl.*, vol. 51, no. 4, pp. 3126–3136, Jul. 2015.

[16] S. Paul and J. Chang, "Fast model-based design of high performance permanent magnet machine for next generation electric propulsion for urban aerial vehicle application," *CES Trans. Electr. Mach. Syst.*, vol. 5, no. 2, pp. 143–151, Jun. 2021.

[17] D. Sun and J. K. Mills, "Development of partial model-based torque control of AC induction motors," *IEEE Trans. Robot. Automat.*, vol. 17, no. 1, pp. 100–107, Feb. 2001.

[18] K. Ahn, A. E. Bayrak, and P. Y. Papalambros, "Electric vehicle design optimization: Integration of a high-fidelity interior-permanent-magnet motor model," *IEEE Trans. Veh. Technol.*, vol. 64, no. 9, pp. 3870–3877, Sep. 2015.

[19] X. Yang, J. Li, H. Miao, and Z. Shi, "Hydraulic pressure control and parameter optimization of integrated electro-hydraulic brake system," SAE Tech. Paper, 2017-01-2516, 2017.

[20] J. Li, X. X. Yang, H. Miao, and Z. Shi, "Co-simulation research of integrated electro-hydraulic braking system," SAE Tech. Paper, 2016-01-1647, 2016.

[21] B.-K. Song, D.-K. Kim, S.-I. Kim, H.-J. Park, G.-H. Lee, and M.-S. Lim, "Comparative study on surface-mounted permanent magnet motors with segmented and connected core for brake system," *IEEE Access*, vol. 8, pp. 167930–167938, 2020.

[22] D. R. Wallace and R. U. Fujii, "Software verification and validation: An overview," *IEEE Softw.*, vol. 6, no. 3, pp. 10–17, May 1989.

[23] D. McCloy and H. Martin, *Control of Fluid Power: Analysis and Design*, 2nd ed. Ellis Horwood, 1980, pp. 75–106.

[24] Z. Q. Zhu, D. Wu, and W. Q. Chu, "Influence of local magnetic saturation on iron losses in interior permanent magnet machines," in *Proc. IEEE Int. Conf. Electr. Mach.*, Sep. 2016, pp. 1822–1827.

[25] Z. Azar, Z. Q. Zhu, and G. Ombach, "Influence of electric loading and magnetic saturation on cogging torque, back-EMF and torque ripple of PM machines," *IEEE Trans. Magn.*, vol. 48, no. 10, pp. 2650–2658, Oct. 2012.

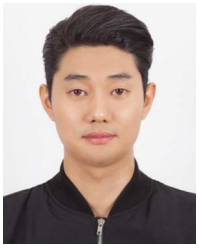

SEON-YEOL OH received the B.S. and M.S. degrees in mechanical engineering from Korea University, Seoul, South Korea, in 2012 and 2014, respectively. Since 2014, he has been working with Mando, Seongnam, South Korea, as a Research Engineer. His research interests include computer-aided analysis of system model and electro-magnetic design of motor.

KYU-YUN HWANG (Member, IEEE) received the B.S. degree in electronic and computer engineering and the Ph.D. degree in electronics, electrical, control and instrumentation engineering from Hanyang University, Ansan-si, South Korea, in 2005 and 2021, respectively. From 2010 to 2012, he was a Research Engineer with Komotek Company Ltd., Seongnam-si, South Korea. Since 2012, he has been a Research Engineer at Mando, Seongnam-si. His research interests include design, analysis, and optimization of electric machines.

BAIK-KEE SONG received the B.S. degree in mechanical engineering and the M.S. degree in automotive engineering from Hanyang University, Seoul, South Korea, in 2009 and 2011, respectively, and the Ph.D. degree in automotive engineering from Hanyang University, in 2022.

Since 2011, he has been working with Mando, Seongnam-si, South Korea, as a Research Engineer. His research interests include electromagnetic design of motor and motor thermal analysis using equivalent circuit.

SUNG-IL KIM (Member, IEEE) received the B.S. and M.S. degrees in electrical engineering from Changwon National University, Changwon, South Korea, in 2003 and 2005, respectively, and the Ph.D. degree in automotive engineering from Hanyang University, Seoul, South Korea, in 2011.

From 2011 to 2017, he was a Research Staff Member with the Samsung Advanced Institute of Technology (SAIT) and a Senior Engineer with the Compressor and Motor Business Team, Samsung Electronics, respectively. Since 2017, he has been an Assistant Professor with the Department of Electrical Engineering, Hoseo University, Asan-si, South Korea. He is the holder of five U.S. patents. His research interests include multi-physics design optimization of electric machines for robot-driven and automotive applications.